論文

Estimation of Lower Limb Joint Angles Using Motion Sensors During Walking and Running[*]

Ayuko SAITO[*1], Yoshikazu KOBAYASHI[*2], Satoru KIZAWA[*2] and Kazuto MIYAWAKI[*2]

This paper describes the use of motion sensors with nine axes to estimate lower limb joint angles during walking and running. Human movement is produced by the rotational motion of the respective joints. Therefore, in an earlier study, the authors estimated knee joint angles by consideration of the centrifugal acceleration and tangential acceleration generated at the thigh and lower leg using motion sensors. For this study, sensor fusion considering centrifugal acceleration and tangential acceleration was applied to estimate the hip, knee, and ankle joint angles in the sagittal plane during walking and running as a first step toward gait analysis using motion sensors. Hip joint flexion and extension were estimated considering the centrifugal acceleration and tangential acceleration caused by three-dimensional rotation of the lumbar. Plantar flexion and dorsiflexion of the ankle joint were estimated considering the centrifugal acceleration and tangential acceleration caused by three-dimensional rotation of the foot. Finally, we evaluated the proposed sensor fusion accuracy for estimation of the lower limb joint angles by comparing the motion sensor results and optical motion capture system results.

Key Words : Joint angle, Lower limb, Running, Sensor fusion, Walking

1. Introduction

Walking, a fundamentally important activity of daily living, is effective for health promotion. Even for frail elderly people, walking helps preserve mobility and independence. Several studies of walking have been conducted from various viewpoints, e.g., simulating walking (1) (2) and measuring gait (3) (4). Particularly, it is important to evaluate walking ability by measuring actual walking accurately because abnormal walking adversely affects activities of daily living. Optical motion capture systems have been used for gait analysis in several studies (5) (6). An optical motion capture system can measure human motion three-dimensionally using retro-reflective markers. Results of other studies have described that optical motion capture systems achieved high accuracy (7) (8). Nevertheless, optical motion capture systems are cumbersome because they require large apparatus. A portable motion capture system is necessary for gait measurement with no location limitation.

＊　原稿受付　令和元年 12 月 23 日．
＊１ 正会員，工学院大学（〒192-0015 東京都八王子市中野町 2665-1）．
＊２ 正会員，秋田工業高等専門学校（〒011-8511 秋田県秋田市飯島文京町 1-1）．

Therefore, compact and lightweight motion sensors have received much attention. A motion sensor comprises a gyro sensor, an acceleration sensor, and a geomagnetic sensor. Several sensor fusion methods for estimating joint angles during exercise have been proposed using information obtained from motion sensors (9) (10). Sensor fusion that corrects drift error of the gyro sensor using the acceleration sensor and geomagnetic sensor is useful for long-term measurements (11) (12). The proportion of the centrifugal acceleration and tangential acceleration in the output of the acceleration sensor increases during exercise because human movement results from rotational motion of the respective joints. Processing signals from the acceleration sensor appropriately in the sensor fusion is important to improve the joint angle estimation accuracy.

For earlier studies, the authors developed a sensor fusion method capable of estimating the knee joint angle during walking by considering the effects of centrifugal acceleration and tangential acceleration. (13) (14). This method can avoid increased observation noise by expressing the centrifugal acceleration and tangential acceleration generated at the thigh and lower leg in the observation equation using angular velocity measurements obtained from the gyro sensor. Accurate estimation of the knee joint angle in the sagittal plane was achieved in earlier studies by considering the centrifugal acceleration and tangential acceleration caused mainly by rotational movement of the thigh and lower leg. Additionally, it is important to measure other lower limb joint angles to evaluate walking ability.

For this study, sensor fusion considering centrifugal acceleration and tangential acceleration is applied to estimate lower limb joint angles in the sagittal plane during walking and running as a first step in gait analysis using motion sensors. The hip joint flexion–extension is estimated considering the centrifugal acceleration and tangential acceleration caused by three-dimensional rotation of the lumbar. Plantar flexion and dorsiflexion of the ankle joint are estimated considering the centrifugal acceleration and tangential acceleration caused by three-dimensional rotation of the foot. Finally, we evaluate the proposed sensor fusion accuracy for estimation of lower limb joint angles by comparing results obtained using sensor fusion and the optical motion capture system.

2. Methods

For this study, Euler angles (roll, pitch, and yaw angles) representing the posture of the nine-axis motion sensors were estimated using sensor outputs. Figure 1 presents the definition of Euler angles of the nine-axis motion sensor. The nine-axis motion sensor (SS-WS1792; Sports Sensing Co., Ltd.) used for this study comprises a three-axis gyro sensor, a three-axis acceleration sensor, and a three-axis geomagnetic sensor. The 38 × 53 × 11 mm sensor weighs 30 g.

The following equations demonstrate how to calculate the initial roll and the initial pitch angles using only acceleration sensor outputs [11] [12].

$$\varphi_A = \arctan\frac{{}^iA_y}{{}^iA_z} \quad \cdots\cdots (1)$$

$$\theta_A = \arctan\frac{-{}^iA_x}{\sqrt{{}^iA_y^2 + {}^iA_z^2}} \quad \cdots\cdots (2)$$

In those equations, ${}^iA_x$, ${}^iA_y$, and ${}^iA_z$ respectively denote the acceleration sensor outputs for x, y, and z axes. Arctangent calculates the inverse tangent of an angle. φ_A and θ_A respectively stand for the initial roll and the initial pitch.

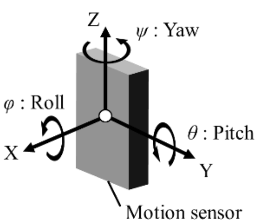

Fig. 1 Definition of Euler angles.

To correct the yaw angle inclination, calculations require the roll φ_A, pitch θ_A, and the geomagnetic sensor outputs [15].

$$\begin{bmatrix} {}^im_x \\ {}^im_y \\ {}^im_z \end{bmatrix} = \begin{bmatrix} \cos\theta_A & \sin\phi_A\sin\theta_A & \cos\phi\sin\theta_A \\ 0 & \cos\phi_A & -\sin\phi_A \\ -\sin\theta_A & \sin\phi_A\cos\theta_A & \cos\phi_A\cos\theta_A \end{bmatrix} \begin{bmatrix} m_x \\ m_y \\ m_z \end{bmatrix} \cdots (3)$$

Therein, m_x, m_y, and m_z respectively stand for the geomagnetic sensor outputs for x, y, and z axes. In addition, ${}^im_x$, ${}^im_y$, and ${}^im_z$ respectively stand for the corrected magnetic fields for the x, y, and z axes. The following equation is used to calculate the initial yaw from the corrected magnetic field.

$$\psi_m = -\arctan\frac{{}^im_y}{{}^im_x} \quad \cdots\cdots (4)$$

Differentials of the roll-pitch-yaw in the absolute coordinate are presented below.

$$\begin{bmatrix} \dot\psi \\ \dot\theta \\ \dot\phi \end{bmatrix} = \begin{bmatrix} 0 & \sin\phi\sec\theta & \cos\phi\sec\theta \\ 0 & \cos\phi & -\sin\phi \\ 1 & \sin\phi\tan\theta & \cos\phi\tan\theta \end{bmatrix} \begin{bmatrix} \omega_x \\ \omega_y \\ \omega_z \end{bmatrix} \quad \cdots\cdots (5)$$

In those matrices, $\dot\phi$, $\dot\theta$, and $\dot\psi$ respectively denote the differentials of the roll–pitch–yaw. Furthermore, ω_x, ω_y and ω_z respectively stand for the gyro sensor outputs for x, y, and z axes. Then the roll–pitch–yaw angles are estimated successively by substituting Eq. (5) into Eq. (6).

$$\begin{bmatrix} \psi \\ \theta \\ \phi \end{bmatrix}_{t+1} = \int \begin{bmatrix} \dot\psi \\ \dot\theta \\ \dot\phi \end{bmatrix}_t dt + \begin{bmatrix} \psi \\ \theta \\ \phi \end{bmatrix}_t \quad \cdots\cdots (6)$$

In that equation, t and t+1 denote times.

For this study, the lower limb joint angles are estimated by considering the effects of centrifugal acceleration and tangential acceleration. Figure 2 shows the rigid link model. Sensor 1 is attached to link i-1; sensor 2 is attached to link i. In addition, r_{i-1} is the vector from the joint of link i-1 to sensor 1; r_i is the vector from the joint of link i to sensor 2. In addition, ω_i and ω_{i-1} respectively denote the angular velocity obtained from the sensor 1 and sensor 2.

The acceleration sensor outputs are translational acceleration, centrifugal acceleration, tangential acceleration,

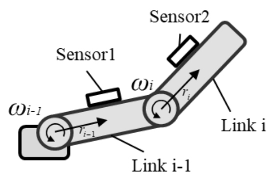

Fig. 2 Rigid link model.

and the acceleration of gravity.

$$A_s = A_{tr} + A_{ct} + g \quad \text{……………………………}(7)$$

In that equation, A_s denotes the acceleration sensor outputs, A_{tr} stands for the translational acceleration, A_{ct} is the sum of the centrifugal acceleration and tangential acceleration, and g represents the acceleration of gravity. The centrifugal acceleration and tangential acceleration are represented using the gyro sensor outputs. Therefore, the respective sums of the centrifugal acceleration and tangential acceleration in link i-1 and link i are the following.

$$A_{ct_{i-1}} = \omega_{i-1} \times \omega_{i-1} \times r_{i-1} + \dot{\omega}_{i-1} \times r_{i-1} \quad \text{………}(8)$$

$$A_{ct_i} = \omega_i \times \omega_i \times r_i + \dot{\omega}_i \times r_i \quad \text{…………………}(9)$$

In those equations, $\omega_{i\text{-}1}$ and ω_i respectively denote the gyro sensor outputs in link i-1 and link i. In addition, $r_{i\text{-}1}$ is the vector from the joint of the link i-1 to sensor 1. Additionally, r_i is the vector from the joint of the link i to the sensor 2. The differentials of gyro sensor outputs are denoted as $\dot{\omega}_{i-1}$ and $\dot{\omega}_i$. Eq. (10) is used to differentiate the gyro sensor outputs.

$$D(s) = \frac{s}{1+ns} \quad \text{…………………………………}(10)$$

In that equation, s is the Laplace operator; n is the time constant. For this study, $n = 0.01$.

The correction formulas of the centrifugal acceleration and tangential acceleration using Eq. (8) and Eq. (9) are

$$A_{s_{i-1}} - A_{ct_{i-1}} = g_{i-1} \quad \text{and} \quad \text{………………………}(11)$$

$$A_{s_i} - A_{ct_i} = {}^{i}R_{i-1}\left(\omega_{i-1} \times \omega_{i-1} \times r_{i-1} + \dot{\omega}_{i-1} \times r_{i-1}\right) + g_i \quad \text{………}(12)$$

where $g_{i\text{-}1}$ and g_i respectively denote the acceleration of gravity in link i-1 and link i. In addition, ${}^{i}R_{i\text{-}1}$ denotes the rotational matrix from the sensor i-1 coordinate system to the sensor i coordinate system. Translational acceleration in link i is represented by the sum of the centrifugal acceleration and tangential acceleration in link i-1. For this study, the translational acceleration of the foot is expressed as the sum of the centrifugal acceleration and tangential acceleration of the lower leg. The translational acceleration of the lower leg is expressed as the sum of the centrifugal acceleration and tangential acceleration of the thigh. The translational acceleration of the thigh is expressed using the translational acceleration and the sum of the centrifugal acceleration and tangential acceleration of the lumbar.

Roll–pitch–yaw angles of the lower limb segments are estimated by sensor fusion using the extended Kalman filter. The nonlinear state equation and the nonlinear measurement equation in link i-1 are shown as Eq. (13) and Eq. (14). The nonlinear state equation and the nonlinear measurement equation in link i are shown in Eq. (15) and Eq. (16).

$$x_{t+1} = F(x_t) + w_t \quad \text{………………………}(13)$$

$$y_t = H(x_t) + v_t \quad \text{………………………}(14)$$

$$x_t = \begin{bmatrix} \psi_{i-1,t} \\ \theta_{i-1,t} \\ \varphi_{i-1,t} \end{bmatrix},$$

$$F(x_t) = \begin{bmatrix} \psi_{i-1,t} + \sin\varphi_{i-1,t}\sec\theta_{i-1,t}\omega_{y_{i-1},t}\cdot Ts + \cos\varphi_{i-1,t}\sec\theta_{i-1,t}\omega_{z_{i-1},t}\cdot Ts \\ \theta_{i-1,t} + \cos\varphi_{i-1,t}\omega_{y_{i-1},t}\cdot Ts - \sin\varphi_{i-1,t}\omega_{z_{i-1},t}\cdot Ts \\ \varphi_{i-1,t} + \omega_{x_{i-1},t}\cdot Ts + \sin\varphi_{i-1,t}\tan\theta_{i-1,t}\omega_{y_{i-1},t}\cdot Ts + \cos\varphi_{i-1,t}\tan\varphi_{i-1,t}\omega_{z_{i-1},t}\cdot Ts \end{bmatrix},$$

$$y_t = \begin{bmatrix} \psi_{m_{i-1},t} \\ A_{x,s_{i-1}} - A_{x,ct_{i-1}} \\ A_{y,s_{i-1}} - A_{y,ct_{i-1}} \\ A_{z,s_{i-1}} - A_{z,ct_{i-1}} \end{bmatrix}, \quad H(x_t) = \begin{bmatrix} \psi_t \\ \left({}^{0}R_{i-1}\right)_t^T \begin{bmatrix} 0 \\ 0 \\ g \end{bmatrix} \end{bmatrix}$$

$$x_{t+1} = F(x_t) + w_t \quad \text{………………………}(15)$$

$$y_t = H(x_t) + v_t \quad \text{………………………………}(16)$$

$$x_t = \begin{bmatrix} \psi_{i,t} \\ \theta_{i,t} \\ \varphi_{i,t} \end{bmatrix},$$

$$F(x_t) = \begin{bmatrix} \psi_{i,t} + \sin\varphi_{i,t}\sec\theta_{i,t}\omega_{y_i,t}\cdot Ts + \cos\varphi_{i,t}\sec\theta_{i,t}\omega_{z_i,t}\cdot Ts \\ \theta_{i,t} + \cos\varphi_{i,t}\omega_{y_i,t}\cdot Ts - \sin\varphi_{i,t}\omega_{z_i,t}\cdot Ts \\ \varphi_{i,t} + \omega_{x_i,t}\cdot Ts + \sin\varphi_{i,t}\tan\theta_{i,t}\omega_{y_i,t}\cdot Ts + \cos\varphi_{i,t}\tan\varphi_{i,t}\omega_{z_i,t}\cdot Ts \end{bmatrix},$$

$$y_t = \begin{bmatrix} \psi_{m_i,t} \\ A_{x,s_i} - A_{x,ct_i} \\ A_{y,s_i} - A_{y,ct_i} \\ A_{z,s_i} - A_{z,ct_i} \end{bmatrix},$$

$$H(x_t) = \begin{bmatrix} \psi_t \\ \left({}^{0}R_i\right)_t^T \begin{bmatrix} 0 \\ 0 \\ g \end{bmatrix} + \left({}^{0}R_i\right)_t^T \cdot \left({}^{0}R_{i-1}\right)_t \cdot \left(\omega_{i-1,t} \times \omega_{i-1,t} \times r_{i-1,t} + \dot{\omega}_{i-1,t} \times r_{i-1,t}\right) \end{bmatrix}$$

In those equations, t and t+1 denote times. In addition, w_t and v_t signify white noise. Furthermore, ${}^{0}R_{i\text{-}1}$ denotes the rotational matrix from the sensor i-1 coordinate system to the absolute coordinates. ${}^{0}R_i$ denotes the rotational matrix from the sensor i coordinate system to the absolute coordinates. Ts represents the sampling period of the nine-axis motion sensors. Partial differentiations of $F(x_t)$ and $H(x_t)$ are the following.

$$f(x_t) = \frac{\partial F(x_t)}{\partial x_t} \quad \text{……………………………}(17)$$

$$h(x_t) = \frac{\partial H(x_t)}{\partial x_t} \quad \text{………………………………}(18)$$

The prediction step (Eqs. (19), (20)) and the filtering step (Eqs. (21)–(23)) are calculated using the nonlinear discrete-time system represented by Eqs. (13)–(18).

$$x_{t+1}^{-} = F(x_t) \quad \cdots\cdots (19)$$

$$P_{t+1}^{-} = f_t P_t f_t^{T} + Q \quad \cdots\cdots (20)$$

$$K_{t+1} = P_{t+1}^{-} h_{t+1}^{T} \left(h_{t+1} P_{t+1}^{-} h_{t+1}^{T} + R \right)^{-1} \quad \cdots\cdots (21)$$

$$x_{t+1} = x_{t+1}^{-} + K_{t+1}\left(y_{t+1} - H\left(x_{t+1}^{-}\right)\right) \quad \cdots\cdots (22)$$

$$P_{t+1} = \left(I - K_{t+1} h_{t+1} \right) P_{t+1}^{-} \quad \cdots\cdots (23)$$

In those equations, P denotes the error covariance matrix, K stands for the Kalman gain, and Q and R respectively represent the covariance matrices of white noise w_t and v_t.

Roll–pitch–yaw angles of each segment obtained from the sensor fusion are converted into the rotational matrix in absolute coordinates using Eq. (24). The rotational matrix from the sensor i coordinate system to the sensor i-1 coordinate system is calculated by substituting Eq. (24) into Eq. (25).

$${}^{o}R_i = \begin{bmatrix} \cos\psi & -\sin\psi & 0 \\ \sin\psi & \cos\psi & 0 \\ 0 & 0 & 1 \end{bmatrix} \cdot \begin{bmatrix} \cos\theta & 0 & \sin\theta \\ 0 & 1 & 0 \\ -\sin\theta & 0 & \cos\theta \end{bmatrix} \cdot \begin{bmatrix} 1 & 0 & 0 \\ 0 & \cos\varphi & -\sin\varphi \\ 0 & \sin\varphi & \cos\varphi \end{bmatrix} \cdots (24)$$

$${}^{i-1}R_i = \left({}^{0}R_{i-1}\right)^{T} \cdot \left({}^{0}R_i\right) = \begin{bmatrix} r_{11} & r_{12} & r_{13} \\ r_{21} & r_{22} & r_{23} \\ r_{31} & r_{32} & r_{33} \end{bmatrix} \quad \cdots\cdots (25)$$

In those equations, r_{mn} (m=1,2,3, n=1,2,3) are the matrix elements of Eq. (25). The following equations demonstrate calculation of Euler angles from the sensor i coordinate system to the sensor i-1 coordinate system using the matrix elements.

$$\psi = arctan \frac{r_{21}}{r_{11}} \quad \cdots\cdots (26)$$

$$\theta = arctan \frac{-r_{31}}{\sqrt{r_{32}^2 + r_{33}^2}} \quad \cdots\cdots (27)$$

$$\varphi = arctan \frac{r_{32}}{r_{33}} \quad \cdots\cdots (28)$$

Therein, ψ, θ, and φ respectively stand for yaw, pitch, and roll from the sensor i coordinate system to the sensor i-1 coordinate system.

3. Experiment

The experiment measured the respective walking and running gaits of three healthy adults: subjects A, B, C. After explanation of the purpose and requirements of the study, the participants gave written informed consent to participation. Study approval was obtained from the Research Ethics Board, National Institute of Technology, Akita College. During the experiment, an optical motion capture system (Bonita 10; Vicon Motion Systems Ltd.), a floor reaction force gauge (9286; Kistler Japan Co. Ltd.), and four nine-axis motion sensors measured the gait. Walking and running speeds were, respectively, about 4.3 km per hour and 7.2 km per hour. The nine-axis motion sensors were attached to the lower limb (lumbar, left thigh, lower left leg, and left foot) of each participant. The sensor positions are depicted in Fig. 3. The sensor attached to the lumbar is situated between the right posterior superior iliac spine and the left posterior superior iliac spine. The definition of the lower limb joint angle is shown in Fig. 4. Anthropometric data are presented in Table 1. The lower limb joint angles in the sagittal plane were calculated using Eq. (27) because the joint angles in the sagittal plane are angles around the Y-axis. The respective sampling frequencies of the nine-axis motion sensors, the optical motion capture system, and the floor reaction force gauge were 100 Hz.

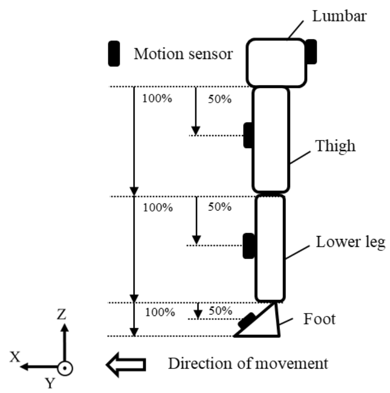

Fig. 3 Setting the sensor position.

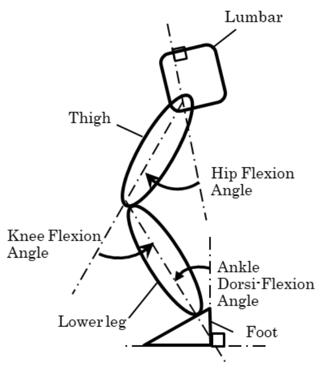

Fig. 4 Definitions of lower limb joint angles.

Table 1 Anthropometric data

Subject	Height [m]	Weight [kg]	Age (years)
Subject A	1.72	65	19
Subject B	1.78	60	19
Subject C	1.63	77	19

4. Results and Discussion

Results for the joint angles (left ankle, left knee, and left hip) of subject A during walking are presented in Fig. 5. Results for the centrifugal and tangential acceleration of subject A during walking are presented in Fig. 6. Results depicted in Fig. 6 are a composite acceleration of centrifugal and tangential acceleration calculated using Eq. (9). The horizontal axis shows the normalized time, where one gait cycle is 100%. The double support phase and the single support phase were found using measurement information obtained from the floor reaction force gauge. Results obtained for the other two participants showed similar tendencies.

The sensor fusion results in Fig. 5 are similar to results obtained using the optical motion capture system. The estimated ankle joint angle showed the peak of plantar flexion in the end of the double support phase and the midpoint of the swing phase. The estimated knee joint angle showed the peak of the flexion in the midpoint of the stance phase and the last half of the swing phase. The estimated hip joint angle showed the peak of the extension early in the swing phase. These characteristics are similar to typical joint angle patterns that are recorded during walking [16].

The sensor attached to lower leg was used for estimating the ankle joint and knee joint angles. Good agreement was found between the ankle joint and knee joint angles obtained from the sensor fusion and the optical motion capture system, although the centrifugal and tangential acceleration obtained from the sensor attached to lower leg changed drastically during the whole gait cycle. In addition, the hip joint angle was estimated accurately, although the centrifugal and tangential acceleration obtained from sensors attached to the thigh and lumbar finely changed in 0–80% of one gait cycle.

Furthermore, results obtained from the sensor fusion and the optical motion capture system were compared to evaluate the sensor fusion accuracy for joint angle estimation. Table 2 presents the root mean square errors (RMSE) between the sensor fusion results and the optical motion capture system results during walking. Averages among all subjects of root mean square error were 5.1 degrees for the ankle joint, 3.0 degrees for the knee joint, and 2.7 degrees for the hip joint. The root mean square errors of the ankle joint were larger than those of the other two joints. The estimation accuracy of the ankle joint angle was presumably reduced because the noise included in the output of the sensor attached to the foot

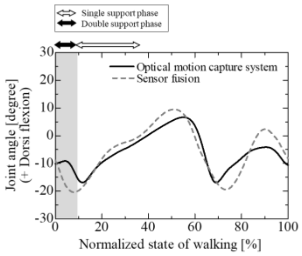

(a) Ankle joint

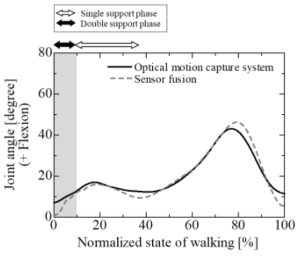

(b) Knee joint

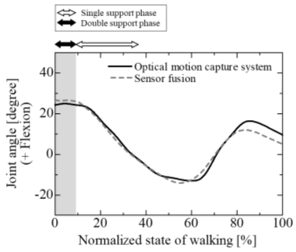

(c) Hip joint

Fig. 5 Lower limb joint angles during walking obtained from the optical motion capture system and the sensor fusion (Subject A).

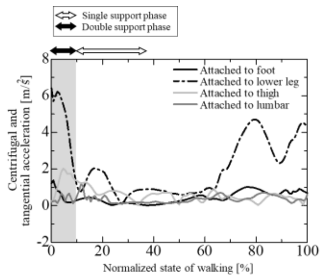

Fig. 6 Centrifugal and tangential acceleration during walking obtained from four sensors attached to lower limb of subject A.

Table 2 Root mean square error of estimated joint angles during walking

Subject	RMSE [degree]		
	Ankle joint	Knee joint	Hip joint
Subject A	4.03	2.67	2.40
Subject B	4.15	2.55	2.92
Subject C	7.14	3.86	2.84

increased as a result of the impact of heel-contact and toe-off. Nevertheless, the waveform of each joint angle estimated by the sensor fusion matched the results obtained from the optical motion capture system.

Results for the joint angles (left ankle, left knee, and left hip) of subject A during running are presented in Fig. 7.

Results for the centrifugal and tangential acceleration of subject A during running are presented in Fig. 8. The results presented in Fig. 8 are a composite acceleration of centrifugal and tangential acceleration calculated using Eq. (9). The horizontal axis shows time, where one cycle is 100%. One cycle extends from heel-contact to the next heel-contact, as determined using the measurement information obtained from the floor reaction force gauge. All results obtained for the other two participants showed similar tendencies.

Centrifugal and tangential acceleration obtained from all sensors were greater than those during walking. Particularly, the centrifugal and tangential acceleration obtained from sensors attached to the lower leg were larger and changed drastically throughout cycle. Although the three joint angles obtained from the sensor fusion were slightly different from the results obtained from the optical motion capture system at the peaks of the plantar and dorsiflexion, or flexion and extension, the waveform of each joint angle estimated from the sensor fusion matched results obtained from the optical motion capture system.

Results from the sensor fusion and the optical motion capture system were compared to evaluate the accuracy of sensor fusion for joint angle estimation. The RMSE between the sensor fusion results and the optical motion capture system results during running are presented in Table 3. The averages among all subjects of root mean square error were 9.6 degrees for the ankle joint, 6.2 degrees for the knee joint, and 7.8 degrees for the hip joint. The root mean square errors of each joint were larger than those during walking. Other factors aside from centrifugal and tangential acceleration presumably affect the estimation accuracy during running because the effect is greater at heel-contact and toe-off than during walking.

5. Conclusions

For this study, lower limb joint angles were estimated using sensor fusion considering the centrifugal acceleration and tangential acceleration generated in the lower limb. During the experiment, the optical motion capture system and four nine-axis motion sensors measured the gait. Lower limb joint angles were estimated using the extended Kalman filter with information obtained from the motion sensors. In the sensor fusion algorithm, translational acceleration of the left foot was expressed using the sum of the centrifugal acceleration and tangential acceleration of the lower leg. The translational acceleration of the lower leg was expressed as the sum of the centrifugal acceleration and tangential acceleration of the thigh. The translational acceleration of the thigh was expressed as the sum of the lumbar centrifugal acceleration and tangential acceleration. Results obtained from the sensor fusion were similar to those obtained from the optical motion capture system during both walking and running. Therefore, the sensor fusion proposed in this study is anticipated for use in estimating entire body posture in sports and healthcare applications. Higher estimation accuracy will

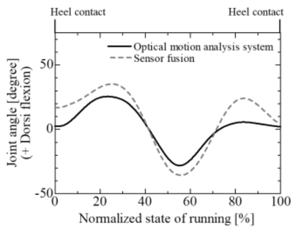

(a) Ankle joint

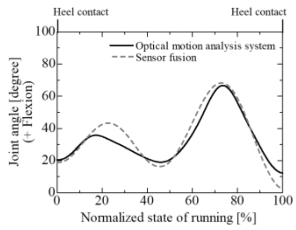

(b) Knee joint

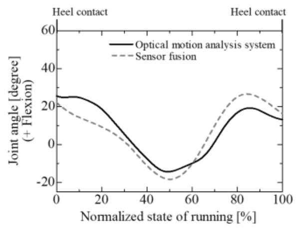

(c) Hip joint

Fig. 7 Lower limb joint angles during running obtained from the optical motion capture system and the sensor fusion (Subject A).

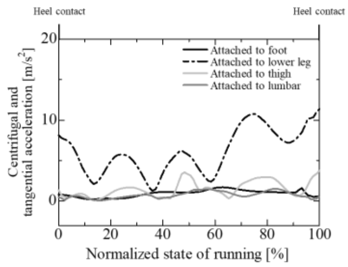

Fig. 8 Centrifugal and tangential acceleration during running obtained from four sensors attached to lower limbs of subject A.

Table 3 Root mean square error of estimated joint angles during running

Subject	RMSE [degree]		
	Ankle joint	Knee joint	Hip joint
Subject A	10.00	5.29	6.63
Subject B	7.14	7.74	7.89
Subject C	11.79	5.69	8.87

necessitate examination of other factors affecting the estimation accuracy measured during running.

References

(1) Maruyama, T. et al., Motion-capture-based walking simulation of digital human adapted to laser-scanned 3D as-is environments for accessibility evaluation, Journal of Computational Design and Engineering, Vol. 3, No. 3 (2016), pp. 250-265.

(2) Hao, M. et al., Effects of hip torque during step-to-step transition on center-of-mass dynamics during human walking examined with numerical simulation, Journal of Biomechanics, Vol. 90, No. 11 (2019), pp. 33-39.

(3) Yamamoto, S., Biomechanics of human movement, Rigakuryoho Kagaku, Vol. 18, No. 3 (2003), pp. 109-114 (in Japanese).

(4) Solomito, M. J. et al., Motion analysis evaluation of adolescent athletes during dual-task walking following a concussion: A multicenter study, Gait & Posture, Vol. 64 (2018), pp. 260-265.

(5) Eggleston, J. D. et al., Analysis of gait symmetry during over-ground walking in children with autism spectrum disorder, J Gait & Posture, Vol. 55 (2017), pp. 162-166.

(6) Oliveira, E. A. et al., Linear and nonlinear measures of gait variability after anterior cruciate ligament reconstruction, Journal of Electromyography and Kinesiology, Vol. 46 (2019), pp. 21-27.

(7) Syam, P. N. et al., A method to calculate the centre of the ankle joint: A comparison with the Vicon® Plug-in-Gait model, Clinical Biomechanics, Vol. 25, No. 6 (2010), pp. 582-587.

(8) Stief, F. et al., Reliability and accuracy in three-dimensional gait analysis: A comparison of two lower body protocols, Journal of Applied Biomechanics, Vol. 29(2013), pp. 105-111.

(9) Hirose, K. et al., Studies of the dynamic analysis and motion measurement of skiing turn using extended Kalman filter, Transactions of the Japan Society of Mechanical Engineers, Series C, Vol. 77, No. 774 (2011), pp. 470-480. (in Japanese).

(10) Saito, A. et al., A study of estimating knee joint angle using motion sensors under conditions of magnetic field variation, Transactions of the JSME (in Japanese), Vol. 85, No. 873 (2019), DOI: 10.1299/transjsme.19-00061.

(11) Vaganay, J. et al., Mobile robot attitude estimation by fusion of inertial data, Proceedings of the IEEE International Conference on Robotics and Automation (1993), pp. 277-282.

(12) Jurman, D. et al., Calibration and data fusion solution for the miniature attitude and heading reference system, Sensors and Actuators, A: Physical, Vol. 138, No. 2 (2007), pp. 411-420.

(13) Saito, A. et al., A study of estimating the knee joint angle during walking using the motion sensors (Focusing on the effect of centrifugal acceleration and tangential acceleration), Transactions of the JSME (in Japanese), Vol. 84, No. 857 (2018a), DOI: 10.1299/transjsme.17-00488.

(14) Saito, A. et al., A study of sensor position for thigh and lower leg motion sensors during walking (Focusing on the knee sagittal plane angle), Transactions of the JSME (in Japanese), Vol. 84, No. 865 (2018), DOI: 10.1299/transjsme.18-00263.

(15) Hirose, K. and Kondo, A., Special Issues No. 3: Measurement Technique for Ergonomics, The Japanese Journal of Ergonomics, Vol. 50, No. 4 (2014), pp. 182-190 (in Japanese).

(16) Yamamoto, H. and Yanagida, Y., The various patterns of knee angle in the stance phase, The Society of Physical Therapy Science, Vol. 26, No. 2 (2011), pp. 269-273 (in Japanese).